International Journal of Solids and Structures 69–70 (2015) 383–391

Contents lists available at ScienceDirect

International Journal of Solids and Structures

journal homepage: www.elsevier.com/locate/ijsolstr

Manipulation of the propagation of out-of-plane shear waves

Linzhi Wu *, Penglin Gao [1]

Center for Composite Materials, Harbin Institute of Technology, Harbin 150001, China

ARTICLE INFO

Article history:
Received 25 October 2014
Received in revised form 4 May 2015
Available online 19 May 2015

Keywords:
Cylindrical cloak
Ray trajectory
Out-of-plane shear wave
Hamiltonian

ABSTRACT

For a given elastic medium, there is a one-to-one correspondence relation between material properties (elastic moduli and density) and the propagation path of elastic waves. Based on this idea, we propose a new method for designing a cylindrical cloak invisible to out-of-plane shear waves. We begin by writing the Hamiltonian governing the path trajectory of out-of-plane shear waves in an inhomogeneous orthotropic medium. Based on Hamilton's equations of motion, we derive the ray equation for out-of-plane shear waves and the differential equation that describes the optimal spatial distribution of material properties in the cylindrical cloak. To solve these two differential equations, two boundary conditions are imposed in terms of the continuity conditions of displacement and traction on the outer boundary of the cylindrical cloak. The two differential equations and two boundary conditions constitute a solvable system from which various cloak profiles can be designed. The proposed approach, which differs from the transformation optics approach, provides an intuitive and flexible design platform and allows considerable freedom to construct invisibility cloaks with a specific spatial distribution of material properties. The effects of the material properties and boundary conditions on cloak invisibility are analyzed in detail. Numerical simulations show that optimized cylindrical cloaks with finite material properties can be easily constructed.

1. Introduction

Pendry et al. (2006) and Leonhardt (2006) independently showed that it is possible to control the paths of electromagnetic waves by changing the spatial distribution of material's properties in the cloak as if nothing is there. Since then, there has been considerable interest in cloaking, and many studies have been devoted to the concept, as recently reviewed by Chen et al. (2010) and Guenneau et al. (2011). To experimentally verify cloak invisibility, a cylindrical cloak was constructed with the use of artificially micro-structured metamaterials and designed to be used at both microwave (Schurig et al., 2006) and optical frequencies (Cai et al., 2007). The concept of cloaking by transformation optics arose from earlier work by Greenleaf et al. (2003a,b), in which push-forward mapping was used to design areas of anisotropic conductivity to make a region undetectable.

Transformation optics has evolved into a powerful tool for the design of invisibility cloaks for electromagnetic waves, acoustic waves, thermal conductivity and electric conductivity. Cummer and Schurig (2007) confirmed the existence of transformation-type solutions for 2D acoustic equations with anisotropic mass and analyzed why the special equivalence of acoustics and electromagnetics occurs only in 2D. A theory of acoustic cloaking was developed using the transformation method for mapping the cloaked region to a point with vanishing scattering strength; the result obtained was that perfect cloaking can be achieved with finite mass through the use of anisotropic stiffness (Norris, 2008). Zhang et al. (2011) presented the practical realization of a low-loss and broadband acoustic cloak for underwater ultrasound in which the metamaterial cloak is constructed with a network of acoustic circuit elements.

Milton et al. (2006) showed that the equations of motion for a general elastic medium are not invariant under coordinate transformations and that if cloaking exists for such classes of waves, it is of a different nature from its electromagnetic and acoustic counterparts. Norris and Shuvalov (2011) generalized the work of Milton et al. (2006), and derived the material properties of the transformed system that depend on the choice of gauge. Colquitt et al. (2014) developed a formal framework for transformation elastodynamics as applied to Kirchhoff–Love plates. It has been demonstrated that the bi-harmonic equation governing the flexural deformation of a linear homogeneous and isotropic Kirchhoff–Love plate is not invariant under general coordinate mapping. Thus, invisibility cloaks can only be designed for certain elastic

* Corresponding author. Tel.: +86 451 86412549; fax: +86 451 86415647.
E-mail address: wlz@hit.edu.cn (L. Wu).
[1] Tel.: +86 451 86412549; fax: +86 451 86415647.

http://dx.doi.org/10.1016/j.ijsolstr.2015.05.012
0020-7683/

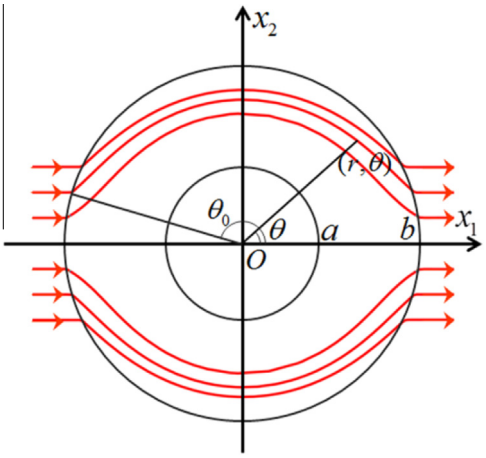

Fig. 1. Path trajectory of an out-of-plane shear wave in the cylindrical cloak. (For interpretation of the references to colour in this figure caption, the reader is referred to the web version of this article.)

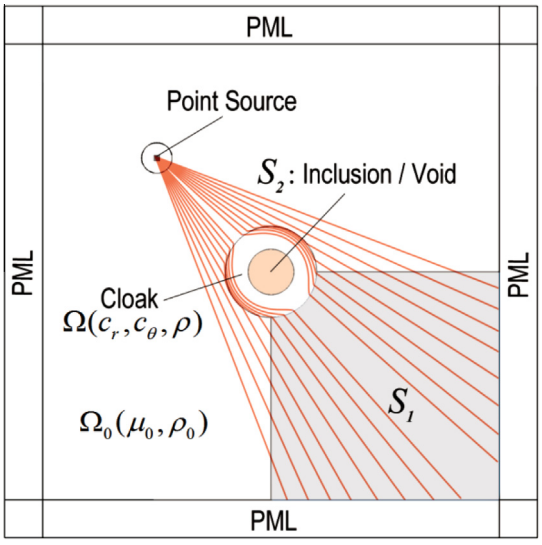

Fig. 2. The black dot at the top left corner denotes a point source, the grey marked area S_1 indicates the integration domain, the red marked area represents an inclusion or a void, and the red rays denote the path trajectories of out-of plane shear waves. (For interpretation of the references to colour in this figure caption, the reader is referred to the web version of this article.)

waves (i.e., antiplane elastic waves) by transformation optics. The extension of the cloaking mechanism to the domain of flexural waves propagating in thin infinite elastic plates has been addressed by adopting a coordinate transformation (Farhat et al., 2009). Brun et al. (2009) proposed a cylindrical cloak designed for fully coupled shear and pressure waves. Following the coordinate transformation, the elastic properties of the cylindrical cloak were derived and its density and elastic moduli with the non-symmetric constitutive tensor were determined. Using the framework of transformation optics, Colquitt et al. (2013) presented a detailed analysis of a physically realizable square cloak for acoustic, out-of-plane shear elastic and electromagnetic waves. Brun et al. (2014) developed a model of a broadband invisibility cloak for channeling flexural waves in thin plates around finite inclusions. Diatta and Guenneau (2014) have investigated spherical cloaks for solid elastic waves using a radially symmetric linear geometric transform. Except for coordinate transformations, the nonlinear elastic pre-stress of neo-Hookean hyperelastic materials has been used as a mechanism to generate finite cloaks and render objects near-invisible to incoming antiplane elastic waves (Parnell et al., 2012). The transformation method in the context of elastic ray theory for high frequency elastic waves has also been examined (Chang et al., 2012). Parnell and Shearer (2013) considered a cloak construction based on the approach of Torrent and Sanchez-Dehesa (2008) and addressed the deviation of the material from neo-Hookean behavior by adopting the arguably more realistic Mooney–Rivlin model. Recently, Schittny et al. (2013) have fabricated macroscopic polymer-based samples with different combinations of small-connection diameter and lattice constant by using three-dimensional printing; they also measured the effective shear and Young's moduli for this type of pentamode metamaterial.

In this paper, our motivation is to propose a new method for determining appropriate material parameters for the cloak by the pre-designed ray trajectory of out-of-plane shear waves. The paper is structured as follows. To design the cloak profile and verify its cloaking performance, we derive the corresponding differential equations and boundary conditions in Section 2 (note that the summation convention over repeated lowercase Latin indices is adopted over the range 1–3). The Hamiltonian for an out-of-plane shear wave is written to describe a propagation path through an inhomogeneous anisotropic medium in Section 2.1. We then derive the ray equation of out-of-plane shear waves through Hamilton's first equation of motion in Section 2.2. The differential equation that governs the spatial distribution of material properties is derived through Hamilton's second equation of motion in Section 2.3. The boundary conditions for the differential equations are given by the interface conditions between the cylindrical cloak and the surrounding medium in Section 2.4. The differential equations are solved and two cloak profiles are used to simulate cloaking performance numerically in Section 2.5. To analyze the scattering of a cylindrical cloak, we employ the scattering measure introduced by Colquitt et al. (2013). In Section 3, two simpler cloak profiles are considered and numerical simulations are provided to demonstrate cloak invisibility. To verify the efficiency of the proposed method, numerical simulations are presented in Section 3.1. In Section 3.2, the effect of boundary conditions (Dirichlet, Neumann and Robin BCs) on cloaking performance is discussed in detail. The effect of soft and hard inclusions on the efficiency of the cloak is examined in Section 3.3. Finally, conclusions from the current study are summarized in Section 4.

2. Design of the cylindrical cloak

Fig. 1 illustrates an inhomogeneous and anisotropic cylindrical cloak Ω with inner radius a and outer radius b. In cylindrical coordinates, the cloak is orthotropic and its elastic moduli are represented by nine independent components of the stiffness tensor: $c_{rrrr}(r)$, $c_{\theta\theta\theta\theta}(r)$, $c_{zzzz}(r)$, $c_{rr\theta\theta}(r) = c_{\theta\theta rr}(r)$, $c_{\theta\theta zz}(r) = c_{zz\theta\theta}(r)$, $c_{zzrr}(r) = c_{rrzz}(r)$, $c_{r\theta r\theta}(r)$, $c_{\theta z\theta z}(r)$ and $c_{zrzr}(r)$. Without loss of generality, a time-harmonic out-of-plane shear wave with unit amplitude $w_0 = e^{i(k_0 x_1 - \omega t)}$ is assumed to be vertically incident on the cylindrical cloak, where $k_0 = \omega/c$ is the wave number in the homogeneous medium Ω_0 outside the cloak, ω is the circular frequency, and c is the speed of the wave in Ω_0. As shown in Fig. 1, symmetric with respect to the x_1-axis allows us to consider only the propagation of the out-of-plane shear wave in the upper half plane satisfying $x_2 \geqslant 0$.

2.1. Hamiltonian and equations of motion

The ray method is often used to study high-frequency wave propagation in inhomogeneous anisotropic media. Let us consider

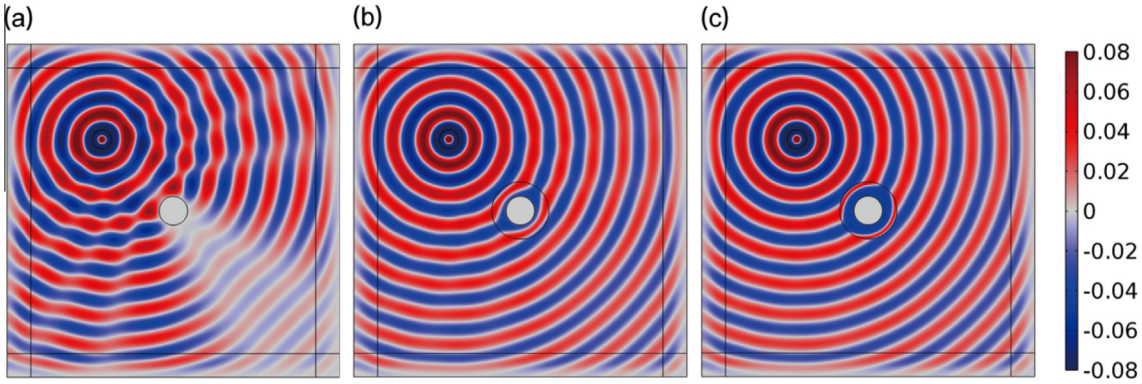

Fig. 3. Snapshots of displacement amplitude field at $\omega = 10$: (a) uncloaked; (b) cloak profile-1; (c) cloak profile-2.

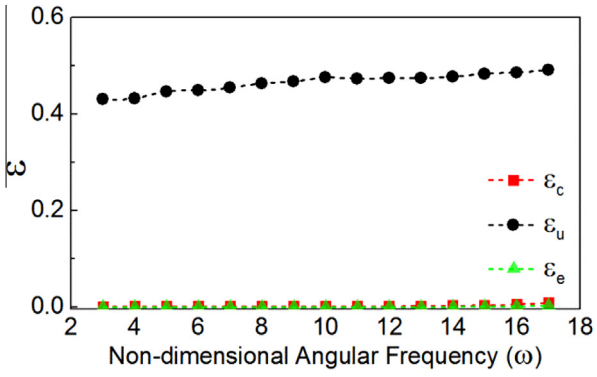

Fig. 4. Variations of scattering measures with non-dimensional angular frequency ω. The green, red and black dashed lines correspond to scattering measures ε_e, ε_c and ε_u, respectively. (For interpretation of the references to colour in this figure caption, the reader is referred to the web version of this article.)

the time-harmonic solution, in which the displacement amplitude field is expanded into a series of inverse powers of frequency ω. Inserting these into the elastodynamic equation yields a polynomial in ω consisting of three terms. The first term, with the highest power of ω, immediately yields the eikonal equation (Cerveny, 2001). Along the path trajectory of out-of-plane shear waves, the eikonal equations can be written, respectively, as

$$c_{i3j3} l_i l_j k_c^2 = \rho_c \omega^2 \quad \text{in } \Omega \tag{1}$$

$$\mu_0 k_0^2 = \rho_0 \omega^2 \quad \text{in } \Omega_0 \tag{2}$$

where c_{ijkl} and ρ_c are the stiffness tensor and density of the cylindrical cloak, respectively, k_c is the norm of the wave vector $\mathbf{k}_c$ in Ω, l_i are the components of the unit vector $\mathbf{l} = \mathbf{k}_c/k_c$, and μ_0 and ρ_0 are the shear modulus and density of the homogeneous medium in Ω_0, respectively. The Hamiltonian governing the path trajectory is essentially the eikonal equation of the out-of-plane shear wave and may be multiplied by an arbitrarily continuous function of spatial coordinates without changing the paths derived from the equations of motion. Eliminating the parameter ω from Eqs. (1) and (2), the Hamiltonian (equivalently, the characteristic equation for the ray) can be expressed as

$$H = \frac{1}{2}[k^2 - n^2(\mathbf{l}, \mathbf{r})] \tag{3}$$

where $k = k_c/k_0$ is the norm of the vector $\mathbf{k} = \mathbf{k}_c/k_0$ and n depends on the Cartesian coordinate $\mathbf{r} = (x_1, x_2, 0)$ and the unit vector $\mathbf{l}$ and can be expressed as

$$n^2 = \frac{\rho}{c_{ij} l_i l_j} \tag{4}$$

where $\rho = \rho_c/\rho_0$ and $c_{ij} = c_{i3j3}/\mu_0$. Because the propagation path of the out-of-plane shear wave is perpendicular to the x_3-axis, we have $l_3 = 0$. Thus, Eq. (4) is related to the non-dimensional parameters c_{11}, c_{22} and $c_{12} = c_{21}$ only.

The path equations in an inhomogeneous anisotropic medium have the form (Cerveny, 2001)

$$\frac{d\mathbf{x}}{d\tau} = \frac{\partial H}{\partial \mathbf{k}} = \mathbf{k} - \frac{1}{2}\frac{\partial n^2}{\partial \mathbf{k}} = \mathbf{s}(\mathbf{k}, \mathbf{x}) \tag{5}$$

$$\frac{d\mathbf{k}}{d\tau} = -\frac{\partial H}{\partial \mathbf{x}} = \frac{1}{2}\frac{\partial n^2}{\partial \mathbf{x}} \tag{6}$$

where $\mathbf{s}$ denotes the ray vector and τ parameterizes the path. The parameter τ is related to the arc length $|d\mathbf{x}|$ by $|d\mathbf{x}| = |\mathbf{s}|d\tau$ where $|\mathbf{s}|$ is the norm of the vector $\mathbf{s}$. For the inhomogeneous anisotropic medium, $\mathbf{s}$ does not coincide with the direction of the normal $\mathbf{k}$ to the phase front.

For the Hamilton's equation of motion shown in Eq. (5), we have the following relation (Kravtsov and Orlov, 1990):

$$s_i = k_i - \frac{\partial n}{\partial l_j}(\delta_{ij} - l_i l_j) \tag{7}$$

where δ_{ij} is the Kronecker delta. Differentiating n^2 in Eq. (4) with respect to l_j and using Eq. (3), we obtain the relation

$$k = n = -\frac{\partial n}{\partial l_j} l_j \tag{8}$$

In the derivation of Eq. (8), we use the fact that the Hamiltonian is equal to zero along the path trajectory. Substituting Eq. (8) and the relation $k_i = k l_i$ into Eq. (7) yields

$$s_i = -\frac{\partial n}{\partial l_i} = \frac{c_{ij} k_j}{c_{pq} l_p l_q} \tag{9}$$

2.2. Path equation of out-of-plane shear waves

Through the coordinate transformation, we have

$$c_{ijkl} = J_{ii'} J_{jj'} J_{kk'} J_{ll'} c_{i'j'k'l'} / \det(J_{mm'}) \quad \text{with} \quad J_{mm'} = \frac{\partial(x_1, x_2, x_3)}{\partial(r, \theta, z)} \tag{10}$$

which represents the derivative of the Cartesian coordinates with respect to the cylindrical coordinates. Eq. (10) gives the transformation relation between the fourth-order tensor in Cartesian coordinates (x_1, x_2, x_3) and the one in cylindrical coordinates (r, θ, z). Substituting $c_r = c_{rzrz}/\mu_0$, $c_\theta = c_{\theta z \theta z}/\mu_0$ and $c_z = c_{zzzz}/\mu_0$ in cylindrical coordinates into Eq. (10), we obtain

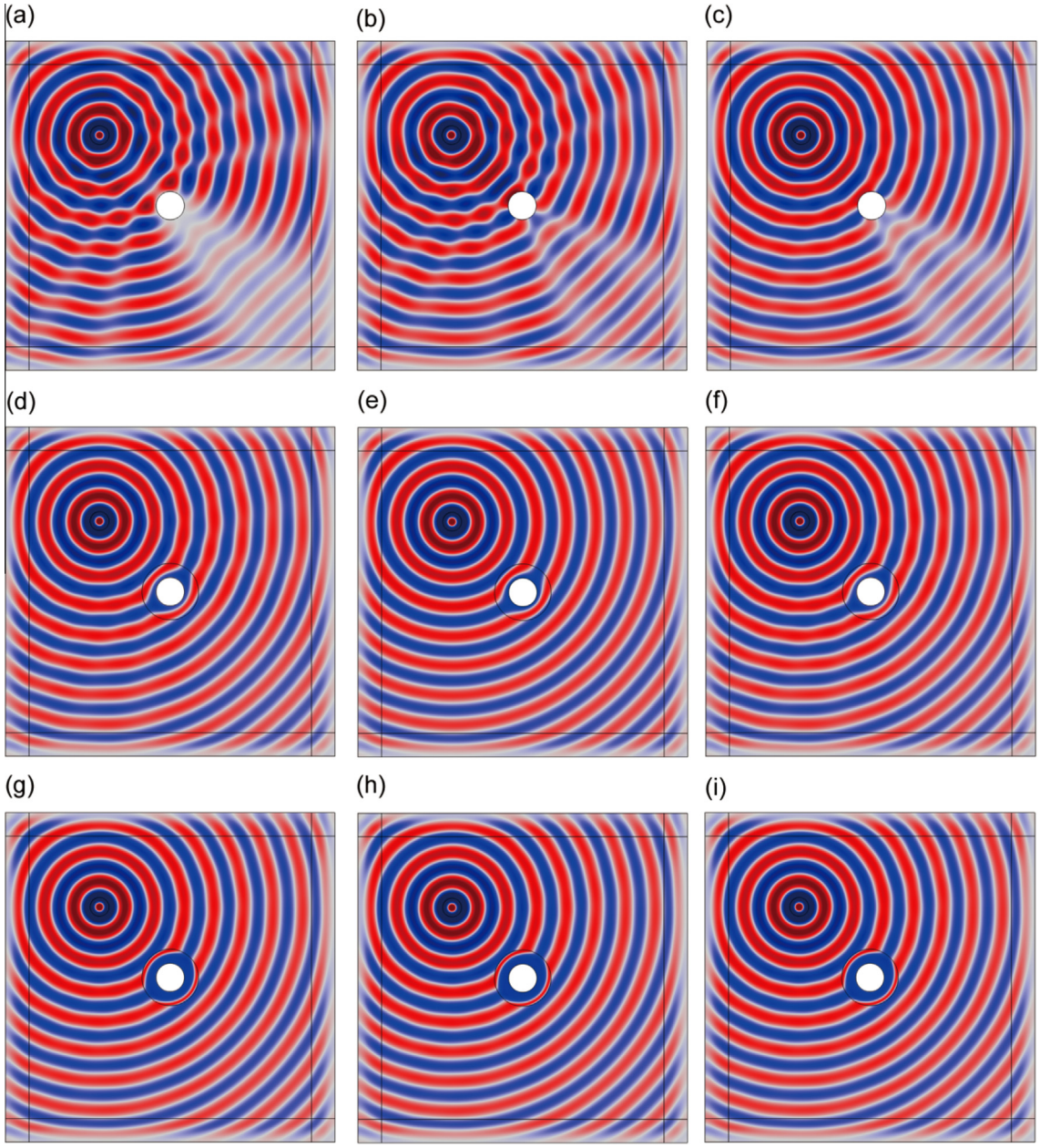

Fig. 5. Snapshots of displacement amplitude field for different cloak profiles and boundary conditions. (a) uncloaked, Dirichlet BC; (b) uncloaked, Neumann BC; (c) uncloaked, Robin BC; (d) CP1, Dirichlet BC; (e) CP1, Neumann BC; (f) CP1, Robin BC; (g) CP2, Dirichlet BC; (h) CP2, Neumann BC; (i) CP2, Robin BC. The color scale is the same as in Fig. 3.

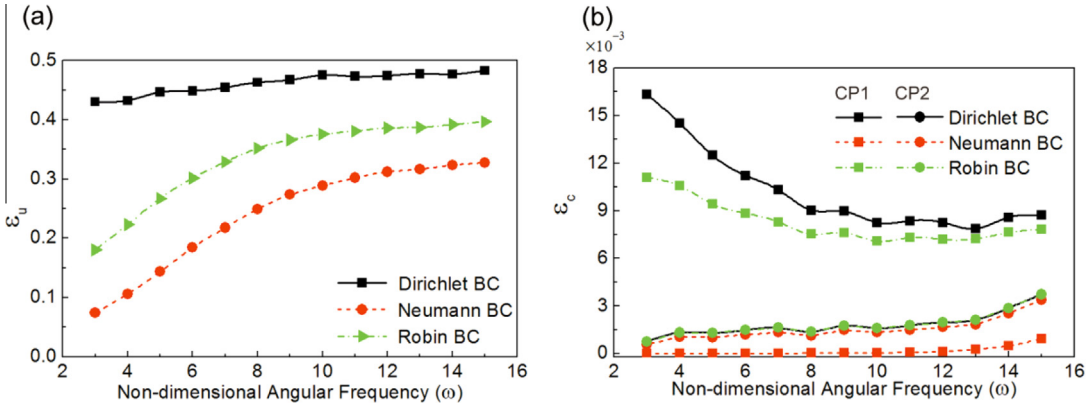

Fig. 6. Variations of scattering measures with ω for different cloak profiles and boundary conditions. (a) uncloaked; (b) cloaked with CP1 and CP2.

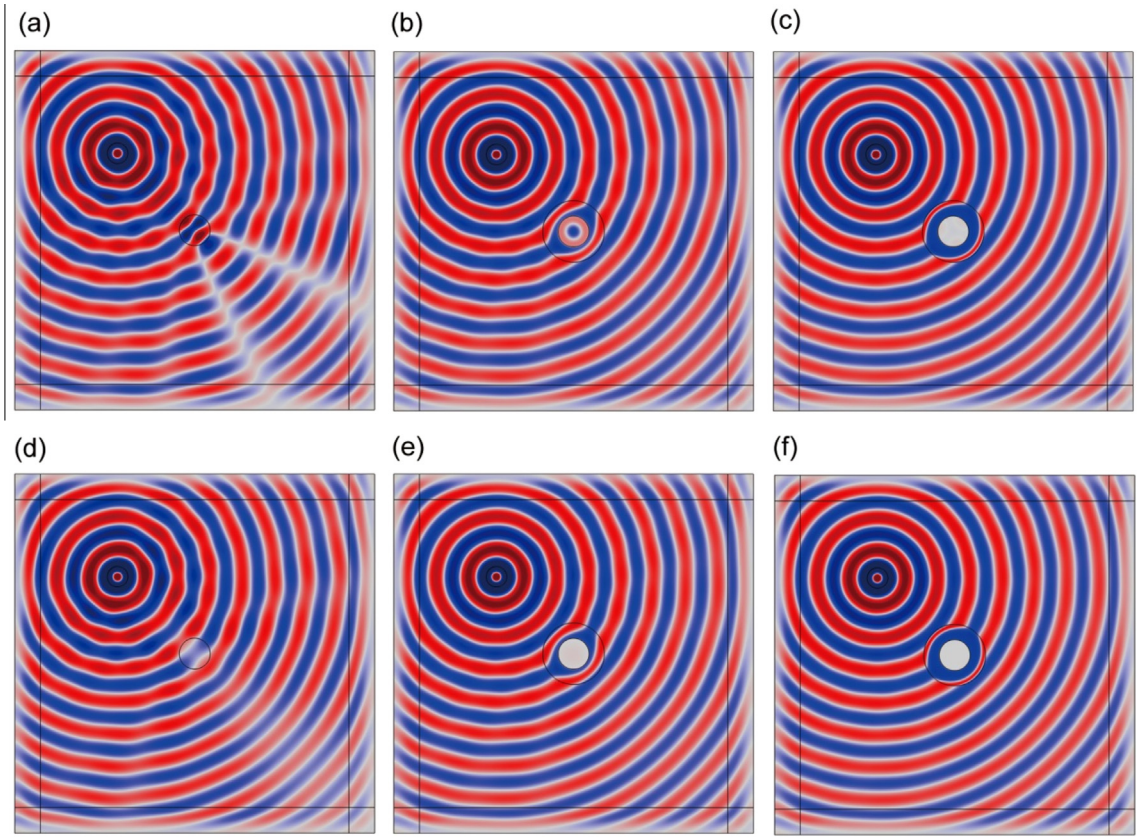

Fig. 7. Snapshots of displacement amplitude field with soft and hard inclusions. (a) soft inclusion, uncloaked; (b) soft inclusion, CP1; (c) soft inclusion, CP2; (d) hard inclusion, uncloaked; (e) hard inclusion, CP1; (f) hard inclusion, CP2. The color scale is the same as in Fig. 3.

Table 1
Variations of scattering measures corresponding to CP1 and CP2 with η under three types of boundary conditions.

ε_c	CP1	CP2		
		$\eta = 3$	$\eta = 4$	$\eta = 5$
Dirichlet BC	8.253×10^{-3}	1.599×10^{-3}	1.078×10^{-3}	1.179×10^{-3}
Neumann BC	4.263×10^{-5}	1.328×10^{-3}	0.898×10^{-3}	1.089×10^{-3}
Robin BC	7.079×10^{-3}	1.598×10^{-3}	1.077×10^{-3}	1.179×10^{-3}

$$c_{11} = c_r\cos^2\theta + c_\theta sin^2\theta, \quad c_{22} = c_r sin^2\theta + c_\theta cos^2\theta, \quad c_{33} = c_z$$
$$c_{12} = c_{21} = (c_r - c_\theta)sin\theta cos\theta, \quad c_{13} = c_{31} = 0, \quad c_{23} = c_{32} = 0 \tag{11}$$

Following the partial derivative of the composite function, the following relations relate the Cartesian coordinates (x_1, x_2, x_3) to the cylindrical coordinates (r, θ, z):

$$\frac{dr}{d\tau} = \frac{dx_1}{d\tau}\cos\theta + \frac{dx_2}{d\tau}\sin\theta \tag{12}$$

$$\frac{rd\theta}{d\tau} = -\frac{dx_1}{d\tau}\sin\theta + \frac{dx_2}{d\tau}\cos\theta \tag{13}$$

Dividing Eq. (12) by Eq. (13) and according to Eqs. (5) and (9), we obtain

$$\frac{dr}{rd\theta} = -\frac{c_r}{c_\theta}\frac{k_1\cos\theta + k_2\sin\theta}{k_1\sin\theta - k_2\cos\theta} \tag{14}$$

Eq. (14) describes the path trajectory of an out-of-plane shear wave that is vertically incident on the cylindrical cloak.

Because the Hamiltonian is equal to zero along the path trajectory, we have, by substituting Eqs. (4) and (11) into Eq. (3)

$$c_r(k_1\cos\theta + k_2\sin\theta)^2 + c_\theta(k_1\sin\theta - k_2\cos\theta)^2 = \rho \tag{15}$$

From Eqs. (14) and (15), we obtain

$$k_1\sin\theta - k_2\cos\theta = \pm\frac{\sqrt{\rho/c_\theta}}{\sqrt{\frac{c_\theta}{c_r}\left(\frac{dr}{rd\theta}\right)^2 + 1}} \tag{16}$$

$$k_1\cos\theta + k_2\sin\theta = \mp\frac{\sqrt{\rho/c_r}}{\sqrt{\frac{c_\theta}{c_r}\left(\frac{dr}{rd\theta}\right)^2 + 1}}\sqrt{\frac{c_\theta}{c_r}}\frac{dr}{rd\theta} \tag{17}$$

As shown in Fig. 1, the out-of-plane shear wave propagates from left to right. Because $\mathbf{k} = (k_1, k_2)$ corresponds to the direction of the normal vector to the phase front and $(\sin\theta, -\cos\theta)$ denotes the unit azimuthal vector along the clockwise direction, the angle between these two vectors is an acute angle. As a result, the right side of Eq. (16) takes a positive sign. From Eqs. (14) and (16), it is easily observed that the right side of Eq. (17) takes a negative sign. Crudo and O'Brien (2009) took the following ray equation for calculating the dielectric tensor:

$$r = a + (b - a)\frac{\sin\theta_0}{\sin\theta} \tag{18}$$

where θ_0 is the incident angle of the out-of-plane shear wave as shown in Fig. 1 and $\sin\theta_0/\sin\theta \leqslant 1$ when $\theta \in [\pi - \theta_0, \theta_0]$. We take this equation as a reference to derive the differential equation of the path trajectory. To obtain a path trajectory equation similar to Eq. (18), we assume using the terms of Eq. (14) that

$$k_1\sin\theta - k_2\cos\theta = f_1(r)\sin\theta \tag{19}$$

Table 2
Energies flowing into soft and hard inclusions for CP1 and CP2.

ω	E (CP1)		E (CP2)	
	Soft	Hard	Soft	Hard
5	8.157×10^{-7}	2.054×10^{-8}	1.835×10^{-8}	7.783×10^{-10}
10	6.843×10^{-5}	4.624×10^{-7}	1.844×10^{-7}	2.738×10^{-9}
15	3.657×10^{-10}	2.524×10^{-6}	6.767×10^{-10}	5.451×10^{-7}

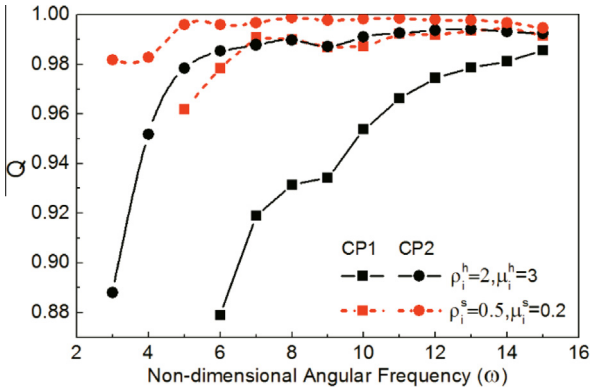

Fig. 8. Variations of the index Q with ω when soft and hard inclusions are present in the cylindrical cloak.

$$k_1 \cos\theta + k_2 \sin\theta = f_2(r)\cos\theta \tag{20}$$

where $f_1(r)$ and $f_2(r)$ are undetermined functions of variable r. From Eqs. (14), (19) and (20), it is found that when $f_1(r) = \sqrt{\rho/c_\theta}$ and $f_2(r) = \sqrt{\rho/c_r}$, we obtain the following relation:

$$\sqrt{\frac{c_\theta}{c_r}}\frac{dr}{rd\theta} = -\frac{\cos\theta}{\sin\theta} \tag{21}$$

2.3. Differential equation of material properties

To derive the differential equation related to the material properties of the cylindrical cloak, we need to use Hamilton's second equation of motion. In cylindrical coordinates, we have

$$\frac{d\mathbf{k}}{d\tau} = \frac{d(k_r\mathbf{e}_r + k_\theta\mathbf{e}_\theta)}{d\tau} \tag{22}$$

where $\mathbf{e}_r$ and $\mathbf{e}_\theta$ are the unit vectors along the radial and azimuthal directions, respectively. Following Auld (1973), we have

$$\frac{d\mathbf{e}_r}{d\tau} = \frac{\partial\mathbf{e}_r}{\partial r}s_r + \frac{\partial\mathbf{e}_r}{r\partial\theta}s_\theta \tag{23}$$

$$\frac{d\mathbf{e}_\theta}{d\tau} = \frac{\partial\mathbf{e}_\theta}{\partial r}s_r + \frac{\partial\mathbf{e}_\theta}{r\partial\theta}s_\theta \tag{24}$$

and

$$\frac{\partial\mathbf{e}_r}{\partial r} = \frac{\partial\mathbf{e}_\theta}{\partial r} = \mathbf{0}, \quad \frac{\partial\mathbf{e}_r}{r\partial\theta} = \frac{1}{r}\mathbf{e}_\theta, \quad \frac{\partial\mathbf{e}_\theta}{r\partial\theta} = -\frac{1}{r}\mathbf{e}_r \tag{25}$$

Substituting Eqs. (23)–(25) into Eq. (22) and comparing it with Eq. (6), we obtain

$$\frac{dk_r}{d\tau} = \frac{1}{2}\frac{\partial n^2}{\partial r} + \frac{k_\theta s_\theta}{r} \tag{26}$$

$$\frac{dk_\theta}{d\tau} = \frac{1}{2}\frac{\partial n^2}{r\partial\theta} - \frac{k_r s_\theta}{r} \tag{27}$$

We can use one of these two expressions to derive the differential equation governing the desired spatial distribution of material properties. We select Eq. (27) to derive the corresponding differential equation. For this purpose, we need to express the differential $d\tau$ in terms of the differential $d\theta$ of the azimuthal angle. Following Kravtsov and Orlov (1990), $d\tau$ can be expressed as

$$d\tau = \frac{|d\mathbf{x}|}{|\mathbf{s}|} = -\frac{1}{|\mathbf{s}|}\sqrt{\left(\frac{dr}{d\theta}\right)^2 + r^2}d\theta \tag{28}$$

The negative sign appears in Eq. (28) because the parameter τ decreases with increasing θ. Substituting Eq. (21) into Eq. (28) and applying Eqs. (9), (19) and (20), we obtain

$$d\tau = -\frac{c_{ij}l_i l_j}{\sqrt{\rho c_\theta}\sin\theta}rd\theta \tag{29}$$

According to the coordinate transformation between the Cartesian coordinates and the cylindrical coordinates, we have from Eqs. (19) and (20)

$$k_r = k_1\cos\theta + k_2\sin\theta = \sqrt{\rho/c_r}\cos\theta \tag{30}$$

$$k_\theta = -k_1\sin\theta + k_2\cos\theta = -\sqrt{\rho/c_\theta}\sin\theta \tag{31}$$

and

$$s_\theta = -s_1\sin\theta + s_2\cos\theta \tag{32}$$

Substituting Eqs. (9) and (11) into Eq. (32) and applying Eqs. (30) and (31), we have

$$s_\theta = -\frac{\sqrt{\rho c_\theta}}{c_{ij}l_i l_j}\sin\theta \tag{33}$$

Differentiating n^2 in Eq. (4) with respect to θ and using Eq. (4), we obtain

$$\frac{\partial n^2}{r\partial\theta} = -\frac{1}{c_{ij}l_i l_j}\left(\frac{\partial c_{pq}}{r\partial\theta}k_p k_q\right) \tag{34}$$

Substituting Eqs. (11), (30) and (31) into Eq. (34), we have

$$\frac{\partial n^2}{r\partial\theta} = \frac{2(c_r - c_\theta)\rho}{rc_{ij}l_i l_j\sqrt{c_r c_\theta}}\sin\theta\cos\theta \tag{35}$$

According to Eq. (21) and substituting Eqs. (29)–(31), (33) and (35) into Eq. (27), we then obtain

$$\frac{1}{\rho/c_\theta}\frac{d(\rho/c_\theta)}{dr} = \frac{2}{r}\left(\sqrt{\frac{c_\theta}{c_r}} - 1\right) \tag{36}$$

Eqs. (21) and (36) form a pair of differential equations that govern the variation of material properties. To obtain expressions for the desired spatial distribution of material properties in the cylindrical cloak Ω, we need to give the corresponding boundary conditions for these two differential equations.

2.4. Interface conditions

To obtain the initial conditions for an out-of-plane shear wave entering the cylindrical cloak, we need to express the continuity conditions of displacement and traction at the interface $r = b$. These can be written as

$$w = w_0, \quad c_{ij3l}\frac{\partial w}{\partial x_l}m_j = \begin{cases} 0 & i \neq 3 \\ i\mu_0 k_0 m_1 & i = 3 \end{cases} \tag{37}$$

where $\mathbf{m} = (\cos\theta_0, \sin\theta_0, 0)$ is the unit normal to the outer surface of the cylindrical cloak. Without loss of generality, the time-harmonic out-of-plane shear wave in the cylindrical cloak can be assumed to be $w = e^{i(\mathbf{k}_c\cdot\mathbf{x}-\omega t)}$. Here, the interface between the background material and the cylindrical cloak is assumed to

be perfectly bonded. For this purpose, the continuity condition of displacement on the interface $r = b$ must be satisfied. Thus, we have the relation $\mathbf{k}_c \cdot \mathbf{x} = \mathbf{k}_0 \cdot \mathbf{x}$ on the interface $r = b$, where $\mathbf{k}_0 = (k_0, 0)$ and $\mathbf{x} = (b\cos\theta_0, b\sin\theta_0)$. From this relation, it is easily derived that the tangential components of vectors $\mathbf{k}_c$ and $\mathbf{k}_0$ along the interface $r = b$ are identical. From Eq. (19), we have the relation $\rho(b)/c_\theta(b) = 1$. Because w is a function of variables x_1 and x_2 and because $m_3 = 0$, the left term in the second expression of Eq. (37) is equal to zero in terms of Eq. (10) when $i \neq 3$. When $i = 3$, we have

$$c_r(k_1\cos\theta_0 + k_2\sin\theta_0) = \cos\theta_0 \tag{38}$$

Obviously, when $\sqrt{c_\theta/c_r} = r/(r-a)$, the path trajectory equation of the out-of-plane shear wave will degenerate into Eq. (18) when the two sides of Eq. (21) are integrated from (b, θ_0) to (r, θ). To extend existing work, however, we consider the more general case of $\sqrt{c_\theta/c_r} = \eta r/(r-a)$ where η is a positive parameter. Letting $r = b$ and $\theta = \theta_0$ in Eq. (20) and according to Eq. (38), we have $\rho(b)c_r(b) = 1$. Thus, the boundary conditions for Eqs. (21) and (36) can be expressed as

$$\frac{\rho(b)}{c_\theta(b)} = 1, \quad \rho(b)c_r(b) = 1 \tag{39}$$

2.5. Cylindrical cloak profiles

For the current problem, we have the relation

$$\frac{c_\theta}{c_r} = \frac{\eta^2 r^2}{(r-a)^2} \tag{40}$$

Substituting Eq. (40) into Eq. (21), we obtain the following path trajectory equation:

$$r = a + (b-a)\left(\frac{\sin\theta_0}{\sin\theta}\right)^{1/\eta} \tag{41}$$

This is the path trajectory equation for the cylindrical cloak. It is easily observed that a singularity for the on-axis ray $(\theta_0 = \pi)$ would arise if it were to traverse the cylindrical cloak (Crudo and O'Brien, 2009). When $\eta = 1$, Eq. (41) is consistent with the path trajectory equation (18). When $\eta \neq 1$, however, Eq. (41) differs from Eq. (18). When η increases, the path trajectory of the out-of-plane shear wave bulges outward. Thus, we can obtain from Eqs. (36), (39) and (40)

$$\frac{\rho}{c_\theta} = \frac{b^2}{(b-a)^{2\eta}}\frac{(r-a)^{2\eta}}{r^2} \tag{42}$$

Eqs. (40) and (42) provide two simple relations that are used to determine the three material parameters c_r, c_θ and ρ. There are many different choices for designing the cylindrical cloak. This flexibility implies that the proposed method can provide different cloak profiles by incorporating multiple simple expressions that satisfy Eqs. (39), (40) and (42). In addition to the shear modulus and density of the cylindrical cloak, the parameter η introduced in the current paper can also be adjusted. Therefore, we have enlarged the design space of the cloak for the case of out-of-plane shear waves, so that it is beneficial for us to make the trade-off between the complexity of material parameters and the cloaking performance. Below, we will consider two specific cloak profiles.

When $\eta = 1$, we take a set of material parameters as follows:

$$c_r = \frac{r-a}{r}, \quad c_\theta = \frac{r}{r-a}, \quad \rho = \left(\frac{b}{b-a}\right)^2\frac{r-a}{r} \tag{43}$$

which satisfy Eqs. (39), (40) and (42). According to the form invariance of the governing equation of out-of-plane shear waves under the coordinate transformation, Parnell and Shearer (2013) also derived material parameters of the cylindrical cloak as shown in Eq. (43). The governing equation of out-of-plane shear waves, which has the same form to that of acoustic waves, is the Helmholtz equation. In this sense, the first application of Eq. (43) was in the work of Cummer and Schurig (2007) on acoustic waves.

As the classical approach to cloaking via coordinate transformation involves deforming a region such that a point is mapped to a finite region corresponding to the inner boundary of the cloak, the material parameters given by Parnell and Shearer (2013) inevitably exhibit a singularity on the inner boundary of the cloak. However, the current paper provides an effective way to design cloak profiles with finite material properties. For example, letting c_θ equal a constant, we obtain the set of finite material parameters

$$c_r = \frac{b}{\eta(b-a)}\left(\frac{r-a}{r}\right)^2, \quad c_\theta = \frac{\eta b}{b-a}, \quad \rho = \frac{\eta b^3}{(b-a)^{2\eta+1}}\frac{(r-a)^{2\eta}}{r^2} \tag{44}$$

From Eq. (44), it can be observed that the material property singularity in c_θ is eliminated, but that singularities still exist for c_r and ρ at the inner boundary of the cylindrical cloak. For convenience, we denote the cloaks shown in Eqs. (43) and (44) as cloak profile-1 (CP1) and cloak profile-2 (CP2), respectively.

2.6. Scattering measure of out-of-plane shear waves

Visual observation, though it provides insight in many circumstances, is still a subjective measure. In a microwave field, radar cross section (RCS) is an effective way to measure far-field scattering. Likewise, we hope to define a quantitative index to objectively measure elastic wave scattering. Obviously, there exist no uniform criteria to define such an index. This paper will adopt the 'scattering measure' defined by Colquitt et al. (2013) to analyze cloak performance quantitatively for a problem described by the same equation of motion. The scattering measure is defined as

$$\varepsilon(w_1, w_2, S_1) = \left(\int_{S_1} |w_1(\mathbf{x}) - w_2(\mathbf{x})|^2 dS_1\right)\left(\int_{S_1} |w_2(\mathbf{x})|^2 dS_1\right)^{-1} \tag{45}$$

where $w_1(\mathbf{x})$ and $w_2(\mathbf{x})$ are any two fields and S_1 is the integral domain outside the cloak. Generally, the scatterer will cause a heavy shadow on its back area. Therefore, we can take the lower right corner area of the cylindrical cloak, relative to the incident direction of the point source, as the integral domain of the scattering measure; this is the grey domain shown in Fig. 2. Three displacement fields are used in the following simulation. They are the undisturbed background field w_b, the cloaked field w_c and the uncloaked field w_u. The undisturbed field excited by a unit point source can be analytically expressed as $w_b(\mathbf{x}) = iH_0^{(1)}(\omega\sqrt{\rho_0/\mu_0}|\mathbf{x} - \mathbf{x}_0|)/4$ by the Green function, where $H_0^{(1)}$ is the zero-order Hankel function of the first kind. The quantities $\varepsilon_c(w_c, w_b, S_1)$ and $\varepsilon_u(w_u, w_b, S_1)$ are defined as the quantitative measure of near-field scattering with and without the cloak, respectively. Thus, the perfect cloak corresponds to vanishing ε_c. The quantity $\varepsilon_e(\tilde{w}_b, w_b, S_1)$ is defined as the quantitative measure of numerical errors, where $\tilde{w}_b$ denotes the undisturbed background field given by the finite element method. Another index, $Q = |1 - \varepsilon_c(w_c, w_b, S_1)/\varepsilon_u(w_u, w_b, S_1)|$, is used to evaluate the relative scattering reduction by introducing a cloak and was proposed by Colquitt et al. (2013).

3. Results and discussion

In Section 2, we considered the vertical incidence of out-of-plane shear waves on the cylindrical cloak, which is parallel to the x_1-axis, and derived the equations related to material property distribution within the cylindrical cloak. From Eqs. (40) and (42), it is easily observed that the shear modulus and density of the cylindrical cloak are functions of the variable r only. Thus, the cylindrical cloak with material parameters governed by Eqs. (39), (40) and (42) is axially symmetric. This symmetry implies that the behavior of such a cylindrical cloak is independent of the incident direction of out-of-plane shear waves. In other words, if an out-of-plane shear wave with horizontal incidence can be perfectly cloaked, then out-of-plane shear waves from other directions in the plane $o - x_1x_2$ can also be perfectly cloaked. All simulations in the current paper are implemented in the PDE module of the finite element software COMSOL Multiphysics with the simulation model shown in Fig. 2.

The cylindrical cloak is located at the center of the simulation domain, and the point source is applied at $(-1.5\,\text{m},\ 1.5\,\text{m})$. Perfectly matched layers are applied on the boundary of the simulation domain to simulate an infinite domain. To facilitate computation, the non-dimensional background material properties are taken as $\mu_0 = \rho_0 = 1$, and other parameters are taken as $\eta = 3$, $a = 0.3m$, $b = 0.6m$. Because a perfect scatterer would cause the maximum disturbance to the background field, it is often chosen to validate the cloak invisibility; for example, one uses a perfect electric conductor for electromagnetic waves, a rigid immovable solid for acoustic waves and a heat insulator for thermal diffusion. For this purpose, the non-dimensional material properties inside the cylindrical cloak are taken as $\mu_i \to \infty$ and $\rho_i \to \infty$. Only the case of $\eta \geqslant 1$ needs to be considered in the following simulations because the cloaking performance of the cylindrical cloak for out-of-plane shear waves deteriorates when $\eta < 1$.

3.1. Validity of the proposed method

Fig. 3(a–c) show displacement amplitude snapshots of out-of-plane shear waves for three cases: (a) uncloaked; (b) cloak profile-1; (c) cloak profile-2, respectively. It can be observed that both CP1 and CP2 exhibit good cloak invisibility when the non-dimensional angular frequency $\omega = 10$. To depict cloak invisibility quantitatively, we need to calculate the scattering induced by the cylindrical cloak with inclusions. Fig. 4 illustrates the variation of the scattering measure with ω. The dashed lines with black, red and green colors correspond to scattering amounts ε_u, ε_c and ε_e, respectively. The non-vanishing ε_e reflects the numerical errors caused by numerical discretization. It can be observed that ε_e increases slightly with increasing non-dimensional angular frequency. This increase is caused by the relatively coarser mesh compared with the wavelength. (We use the same mesh for different wavelengths in the finite element calculations.) The near-overlap of the two curves corresponding to ε_e and ε_c demonstrates the utility of cloak profile-2.

3.2. Effect of boundary conditions (BC)

The perfect scatterer is often chosen to validate cloak invisibility, but it is also necessary to consider the effect of boundary conditions on the scattering measure. Recently, Jones et al. (2015) analyzed the influence of boundary conditions on the interior surface of the cloaking layer in detail, based on the explicit analytical solutions of a wave propagation problem for a membrane as well as a Kirchhoff flexural plate. In fact, the discussion of boundary conditions illuminates the similarities and differences between cloak profile-1 and cloak profile-2. The current paper considers three types of boundary conditions: rigid boundary, free boundary and impedance boundary. They correspond to the Dirichlet, Neumann and Robin BCs in partial differential equations, respectively. For Robin-type boundary conditions, the ratio of interface impedance $\beta = 1/\sqrt{6}$ is used in numerical simulations of the displacement amplitude field. Fig. 5(a–i) show displacement amplitude snapshots of out-of-plane shear waves for three types of cloaks: (a–c) uncloaked; (d–f) CP1; (g–i) CP2 and for three types of boundary conditions: (a,d,g) Dirichlet BC; (b,e,h) Neumann BC; (c,f,i) Robin BC. From these figures, it can be observed that both CP1 and CP2 exhibit good invisibility for all three boundary conditions mentioned above. To compare the effect of three types of boundary conditions on cloak invisibility, we analyze the corresponding scattering measures quantitatively.

Fig. 6(a and b) illustrate the scattering measures plotted against the non-dimensional angular frequency ω for three types of cloaks and three types of boundary conditions mentioned above, respectively. From Fig. 6(a), it can be observed that ε_u increases with increasing ω, particularly for the Neumann and Robin BCs. In addition, the rigid and free boundaries induce the maximum and minimum scattering, respectively, and the scattering caused by the impedance boundary lies between the two. This finding implies that scattering decreases with the weakening of boundary constraints, which is an intuitive result. Fig. 6(b) demonstrates the difference between CP1 and CP2 for the three types of boundary conditions. The scattering of CP2 is not sensitive to a change in boundary conditions and varies only slightly with increasing ω. When $\omega > 12$, the slight increase in ε_c is caused by the relatively coarser mesh compared with the wavelength. Unlike CP2, the scattering of CP1 is far more sensitive to a change in boundary condition. As shown in Fig. 6(b), CP1 provides an improved degree of invisibility for the free boundary compared to the rigid and impedance boundaries.

The propagation of an out-of-plane shear wave in a cylindrical cloak can be represented by a similar path equation to Eq. (41) (red rays shown in Fig. 1). It is easily found that the path trajectories tend toward the outer boundary of the cylindrical cloak with increasing η. That is, only a small amount of energy propagates through the region near the inner boundary of the cylindrical cloak. Therefore, the inner boundary of the cylindrical cloak decreases the amount of scattering in the propagation of out-of-plane shear waves with increasing η. It is not difficult to understand the sensitivity difference of the inner boundaries corresponding to CP1 and CP2. Table 1 shows the variation of scattering measures with η for three types of boundary conditions. From Table 1, it can be found that scattering measures for three types of boundary conditions tend to the same value with increasing η. This result verifies the validity of the previous analysis.

3.3. Effect of inclusions

The previous section discussed the effect of boundary conditions on cloak invisibility in detail. The rigid and free boundaries are two extreme cases in which the elastic wave cannot propagate across the boundary. However, the impedance boundary lies between these two extreme cases and for this case the elastic wave can propagate across the boundary. For electromagnetic waves, we pay more attention to the disturbed field outside the cloak, as it corresponds to device stealth in practice. For elastic waves, however, except for the cloak and its external region, we also focus on the region inside the cloak because of the potential application of seismic protection.

Here, we consider two typical cases in which the region inside the cylindrical cloak is filled with soft and hard inclusions,

respectively. The non-dimensional material properties of the inclusions are taken as $\rho_i^s = 0.5$, $\mu_i^s = 0.2$ (soft inclusions) and $\rho_i^h = 2$, $\mu_i^h = 3$ (hard inclusions). Fig. 7(a–f) illustrate the displacement amplitude snapshots for the following three cases: (a,d) uncloaked; (b,e) CP1; (c,f) CP2, when the region inside the cloak is filled with two types of inclusions: (a–c) soft inclusions; (d–f) hard inclusions. From Fig. 7(b,c,e,f), it can be observed that CP2 performs well in both cases, whereas CP1 with soft inclusions exhibits poor performance because more energy flows into the inclusions. For narrative convenience, we introduce a parameter $E = \int_{S_2} |w_i(\mathbf{x})|^2 dS_2$, where S_2 is the inclusion area inside the cylindrical cloak and $w_i(\mathbf{x})$ denotes the displacement field in the inclusion, which can be used to approximate the energy flowing into the inclusion. Numerical results in Table 2 show that CP2 can effectively prevent elastic energy from flowing into the inclusion. The disturbed field outside the cloak can still be evaluated by Q, as shown in Fig. 8. It can be observed that the degree of invisibility of the cylindrical cloak strongly improves with increasing ω. In comparison with CP1, CP2 performs better and cloak invisibility is relatively less affected by the material properties of inclusions.

4. Conclusions

Based on the ray tracing idea, we present a new method to design a cylindrical cloak that is effectively invisible to out-of-plane shear waves. The Hamiltonian of the out-of-plane shear wave is used to derive differential equations (21) and (36), which govern the ideal spatial distribution of material properties within the cylindrical cloak. Based on the boundary conditions expressed in Eq. (39), the solutions of Eqs. (21) and (36) can be represented by the two simple expressions (40) and (42). The proposed method can provide different cloak profiles by selecting from many simple expressions that satisfy Eqs. (39), (40) and (42), and the design space is thus enlarged for the case of a cylindrical cloak exposed to out-of-plane shear waves. These results are expected to facilitate the design, fabrication and verification of such cloaks.

To analyze the effects of material properties and boundary conditions on cloak invisibility, we consider three types of boundary conditions on the inner boundary of the cylindrical cloak, along with three types of cloaks. Numerical results show that both CP1 and CP2 exhibit good invisibility for the three types of boundary conditions. The scattering of CP2 is insensitive to changes in the inner boundary of the cylindrical cloak, and its performance is superior to that of CP1 as a whole. Numerical results in Table 2 show that CP2 can effectively prevent elastic energy from flowing into the cloaked object. This result is expected to offer design inspiration in the area of seismic protection.

It should be noted that the proposed approach is based on the asymptotic high-frequency solution of the elastodynamic equation, which requires the appropriate material properties of the medium to not vary greatly over distances on the order of the wavelength. The validity conditions of the ray method have been discussed by Cerveny (2001).

Acknowledgment

This work is supported by National Science Foundation of China under Grant No. 11072068.

References

Auld, B.A., 1973. Acoustic Fields and Waves in Solids. John Wiley & Sons, New York, USA, p. 211.
Brun, M., Guenneau, S., Movchan, A.B., 2009. Achieving control of in-plane elastic waves. Appl. Phys. Lett. 96, 061903.
Brun, M., Colquitt, D.J., Jones, I.S., Movchan, A.B., Movchan, N.V., 2014. Transformation cloaking and radial approximations for flexural waves in elastic plates. New J. Phys. 16, 093020.
Cai, W.S., Chettiar, U.K., Kildishev, A.V., Shalaev, V.M., 2007. Optical cloaking with metamaterials. Nat. Photon. 1, 224–227.
Cerveny, V., 2001. Seismic Ray Theory. Cambridge University Press, New York, USA.
Chang, Z., Liu, X.N., Hu, G.K., Hu, J., 2012. Transformation ray method: controlling high frequency elastic waves (L). J. Acoust. Soc. Am. 132, 2942–2945.
Chen, H.Y., Chan, C.T., Sheng, P., 2010. Transformation optics and metamaterials. Nat. Mater. 9, 387–396.
Colquitt, D.J., Jones, I.S., Movchan, N.V., Movchan, A.B., Brun, M., Mcphedran, R.C., 2013. Making waves round a structured cloak: lattices, negative refraction and fringes. Proc. Roy. Soc. Ser. A 469, 20130218.
Colquitt, D.J., Brun, M., Gei, M., Movchan, A.B., Movchan, N.V., Jones, I.S., 2014. Transformation elastodynamics and cloaking for flexural waves. J. Mech. Phys. Solids 72, 131–143.
Crudo, R.A., O'Brien, J.G., 2009. Metric approach to transformation optics. Phys. Rev. A 80, 033824.
Cummer, S.A., Schurig, D., 2007. One path to acoustic cloaking. New J. Phys. 9, 1–8.
Diatta, A., Guenneau, S., 2014. Controlling solid elastic waves with spherical cloaks. Appl. Phys. Lett. 105, 021901.
Farhat, M., Guenneau, S., Enoch, S., Movchan, A.B., 2009. Cloaking bending waves propagating in thin elastic plates. Phys. Rev. B 79, 033102.
Greenleaf, A., Lassas, M., Uhlmann, G., 2003a. On nonuniqueness for Calderon's inverse problem. Math. Res. Lett. 10, 685–694.
Greenleaf, A., Lassas, M., Uhlmann, G., 2003b. Anisotropic conductivities that cannot be detected by EIT. Physiol. Meas. 24, 413–419.
Guenneau, S., McPhedran, R.C., Enoch, S., Movchan, A.B., Farhat, M., Nicorovici, N.P., 2011. The colours of cloaks. J. Opt. 13, 024014.
Jones, I.S., Brun, M., Movchan, N.V., Movchan, A.B., 2015. Singular perturbations and cloaking illusions for elastic waves in membranes and Kirchhoff plates. arXiv: 1516853.
Kravtsov, Y.A., Orlov, Y.I., 1990. Geometrical Optics of Inhomogeneous Media. Springer, NewYork, USA, pp. 236–238.
Leonhardt, U., 2006. Optical conformal mapping. Science 312, 1777–1780.
Milton, G.M., Briane, M., Willis, J.R., 2006. On cloaking for elasticity and physical equations with a transformation invariant form. New J. Phys. 8, 248–267.
Norris, A.N., 2008. Acoustic cloaking theory. Proc. Roy. Soc. Ser. A 464, 2411–2434.
Norris, A.N., Shuvalov, A.L., 2011. Elastic cloaking theory. Wave Motion 48, 525–538.
Parnell, W.J., Shearer, T., 2013. Antiplane elastic wave cloaking using metamaterials, homogenization and hyperelasticity. Wave Motion 50, 1140–1152.
Parnell, W.J., Norris, A.N., Shearer, T., 2012. Employing pre-stress to generate finite cloaks for antiplane elastic waves. Appl. Phys. Lett. 100, 171907.
Pendry, J.B., Schurig, D., Smith, D.R., 2006. Controlling electromagnetic fields. Science 312, 1780–1782.
Schittny, R., Buckmann, T., Kadic, M., Wegener, M., 2013. Elastic measurements on macroscopic three-dimensional pentamode metamaterials. Appl. Phys. Lett. 103, 231905.
Schurig, D., Mock, J.J., Justice, B.J., Cummer, S.A., Pendry, J.B., Starr, A.F., Smith, D.R., 2006. Metamaterial electromagnetic cloak at micro frequencies. Science 314, 977–980.
Torrent, D., Sanchez-Dehesa, J., 2008. Acoustic cloaking in two dimensions: a feasible approach. New J. Phys. 10, 063015.
Zhang, S., Xia, C.G., Fang, N., 2011. Broadband acoustic cloak for ultrasound waves. Phys. Rev. Lett. 106, 024301.